Supplementary Information

Synergy of CuO/C_3N_4 interface and CuO nanoparticles in the ethynylation of formaldehyde for 1,4-Butynediol synthesis

Wei Sun *[a] Lifeng Cui [a] and Danyang Zhou [b]

[a] Shandong Hualu-Hengsheng Chemical Co., Ltd., Dezhou 253024, China. E-mail: sunwei_qust@163.com.

[b] Key Laboratory of Colloid and Interface Chemistry, Ministry of Education, School of Chemistry and Chemical Engineering, Shandong University, Jinan 250100, China.

1. Materials and methods

1.1 Chemicals:

The chemicals were used as received without further purification: Melamine (99%), Copper (II) nitrate trihydrate ($Cu(NO_3)_2 \cdot 3H_2O$, ≥99 %), Disodium carbonate (Na_2CO_3,≥99.8%), N,N-Dimethylformamide (DMF, ≥99.0%) were obtained from Sinopharm Chemical Reagent. Trimesic acid (BTC, ≥99.0%), Bismuth nitrate pentahydrate ($Bi(NO_3)_3 \cdot 5H_2O$, ≥99.0%) were obtained from Aladdin Biochemical Technology. All aqueous solutions were prepared using deionized water.

1.2 Characterizations:

X-ray photoelectron spectroscopy (XPS) analysis was performed on the Thermo Scientific ESCA Lab 250Xi using 200 W monochromatic Al Kα radiation. The 500 μm X-ray spot was used. The base pressure in the analysis chamber was about 3×10-10 mbar. Typically, the hydrocarbon C1s line at 284.8 eV from adventitious carbon was used for energy referencing. X-ray diffraction (XRD) analysis of the samples was performed on the X-ray diffractometer (Model D/MAX2500, Rigaka) with Cu-Kα radiation at the scan speed was 5° min^{-1}. The morphologies of the as-synthesized materials were characterized by a HITACHI S-4800 scanning electron microscope (SEM) and a JEOL JEM-2100 Transmission electron microscopy (TEM) with an accelerating voltage of 200 kV. The Cu concentrations of the as-prepared Cu nanoparticles and corresponding Cu-CN catalysts were measured by the inductively coupled plasma optical emission spectroscopy (ICP-OES, Vista-MPX).

1.3 Catalyst synthesis:

synthesis *g-C_3N_4 nanosheets.* In accordance with the described in previous literature,[1] a quantity of 20 g of melamine was contained within a covered crucible and subjected to heating at a rate of 5 °C per minute to a temperature of 550 °C, where it was maintained for a duration of 4 hours within a muffle furnace. The resulting products were subsequently ground into a fine powder and subsequently underwent a second calcination process at 500 °C with a heating rate of 5 °C per minute for an additional 2 hours in an open crucible. The material was then allowed to cool to ambient room temperature, ultimately yielding a yellow powder.

Synthesis of Cu-BTC: The synthesis of Cu-BTC was executed in accordance with the procedure detailed in a preceding report.[2] The Cu-BTC nanosheets were produced through the complexation reaction between Cu^{2+} ions and BTC in a solution of DMF. Specifically, BTC (2.1 g, 0.01 mol) and $Cu(NO_3)_2 \cdot 3H_2O$ (7.3 g, 0.03 mol) were dissolved in 300 mL of DMF and the mixture was stirred at 80 °C for 24 hours. Following this, the resultant solution was subjected to centrifugation, washing, and drying processes to yield the light blue-colored Cu-BTC nanosheets.

Synthesis of CB/CN-BTC catalyst. In the standard preparation protocol, g-C_3N_4 nanosheets (0.5 g), Cu-BTC (0.5 g), and $Bi_2(NO_3)_3 \cdot 5H_2O$ (0.02 g, 0.04 mmol) were combined in a mortar. The mixture was thoroughly ground to ensure uniform distribution of the components. Subsequently, the blended powder was subjected to calcination in a stream of air at temperatures of 350 °C and 450 °C for a duration of 4 hours. The calcined samples were designated as CB/CN-BTC-350 and CB/CN-BTC-450, respectively, with the nomenclature reflecting the specific calcination temperature employed.

Synthesis of CB-BTC catalyst: The synthesis of CB-BTC nanosheets adhered to a procedure analogous to that of the CB/CN-BTC catalyst, with the exception that g-C3N4 was not required. A homogeneous mixture of Cu-BTC (0.5 g) and $Bi_2(NO_3)_3 \bullet 5H_2O$ (0.02 g) was subjected to calcination in an ambient air atmosphere at a temperature of 350 °C for a duration of 4 hours, thereby yielding the CB-BTC catalyst.

Synthesis of C/CN-BTC-350 catalyst. The synthesis of C/CN-BTC-350 catalyst adhered to a procedure analogous to that of the CB/CN-BTC catalyst, with the exception that $Bi_2(NO_3)_3 \cdot 5H_2O$ was not required. A homogeneous mixture of Cu-BTC (0.5 g) and g-C_3N_4 nanosheets (0.5 g), was subjected to calcination in an ambient air atmosphere at a temperature of 350 °C for a duration of 4 hours, thereby yielding the CB-BTC catalyst.

Table S1 List of abbreviations

Abbreviation	Meaning
BYD	1,4-Butynediol
M NPs	metal nanoparticles
CuC≡CCu	active cuprous species
MOFs	metal-organic frameworks
BTC	1,3,5-benzenetricarboxylate
CB	CuO/Bi_2O_3 nanoparticles
CB-BTC	CuO/Bi_2O_3 NPs catalyst without support
CB/CN-BTC	CuO/Bi_2O_3 NPs co-loaded g-C3N4 catalysts
CB/CN-BTC-350	calcination temperature at 350 ^oC
CB/CN-BTC-450	calcination temperature at 450 ^oC
CB/CN-BTC-F	CB/CN-BTC catalyst activated in formaldehyde system.
CB/CN-BTC-F/A	CB/CN-BTC catalyst activated in formaldehyde/acetylene system

2. Structure and composition of catalysts

Table S2 Composition and structure of catalysts

Catalyst	CuO/%	Bi_2O_3/%	C/%	N/%	CuO Crystal Size/nm
CB-BTC	54.2.	2.5	43.2	-	26.9
CB/CN-BTC-350	42.1	2.2	30.7	24.9	10.8
CB/CN-BTC-450	52.7	2.9	37.5	6.8	20.1

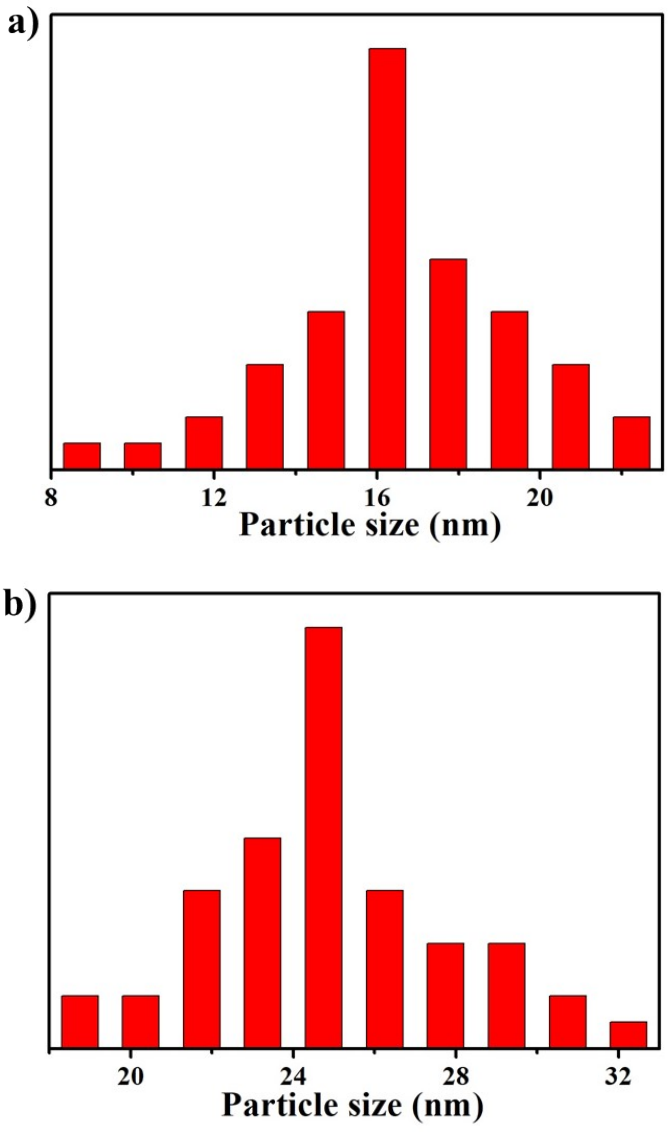

Fig. S1. The histogram of CuO particle size of (a) CB/CN-BTC-350 and (b) CB/CN-BTC-450 catalysts

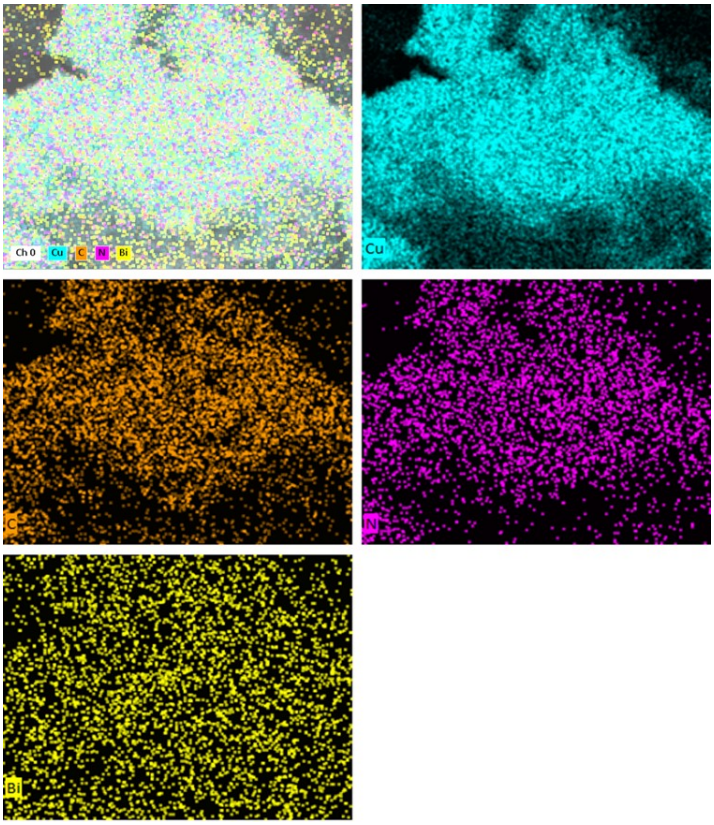

Fig. S2. EDS mapping of the CB/CN-BTC-350 catalyst.

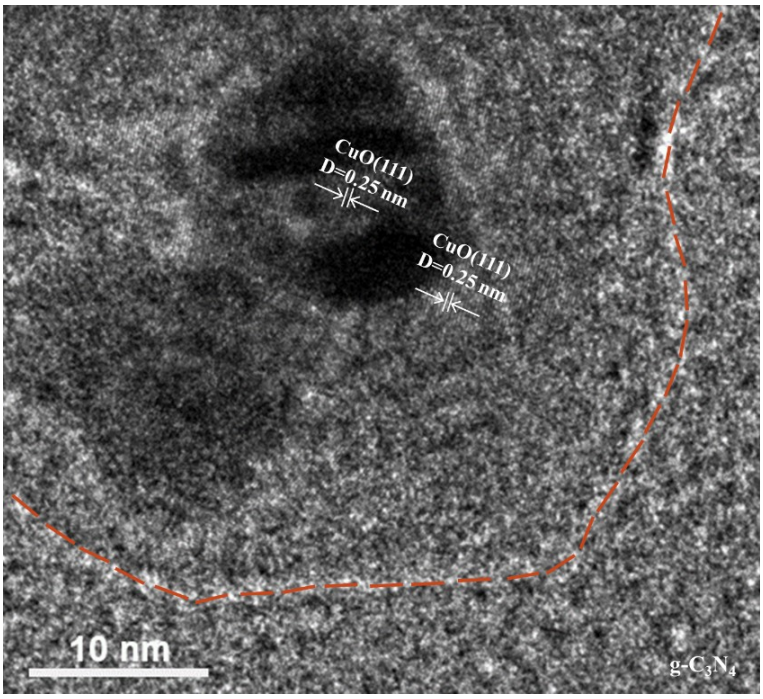

Fig. S3 HR-TEM images of CB/CN-BTC-350 catalyst.

Table S3. Peak position and peak area ratio of different elements and valence states.

Catalysts	Cu(eV)		Cu^{2+}/Cu^{+}
	$Cu^{+}2p_{3/2}$	$Cu^{2+}2p_{3/2}$	(Atomic)
CB/CN-BTC-350	933.3	934.9	0.73
CB/CN-BTC-450	932.5	933.6	1.33

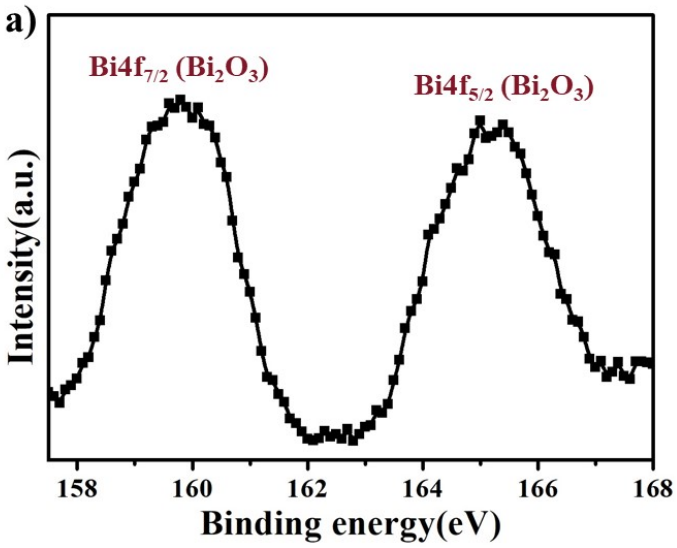

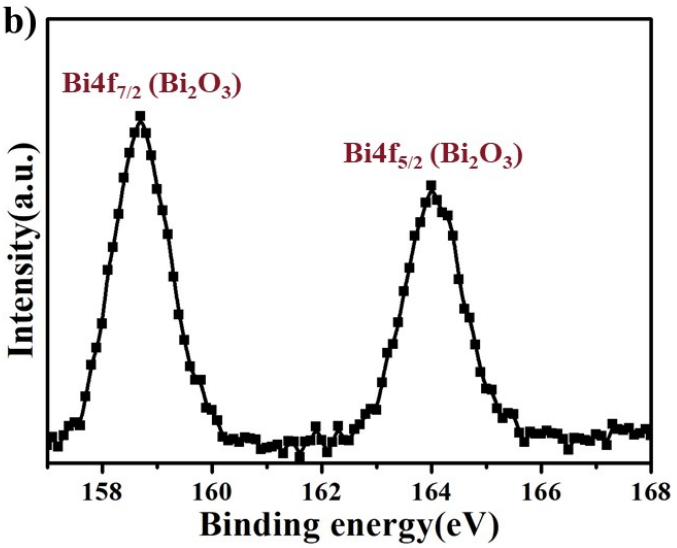

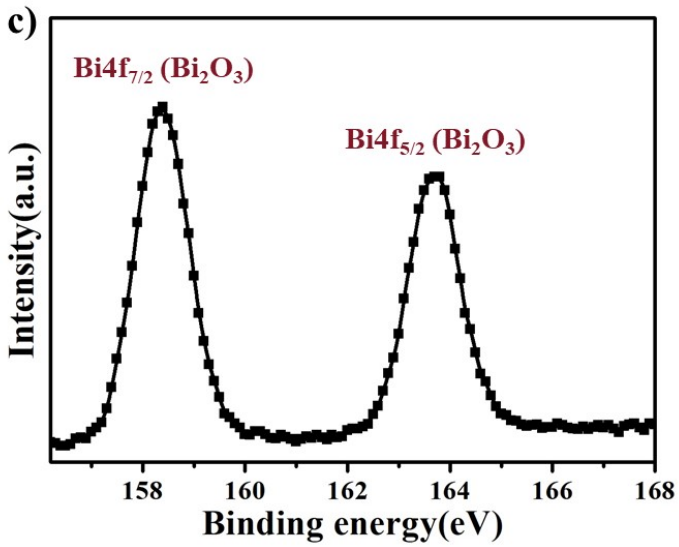

Fig. S4. XPS spectra of Bi 4f peaks of prepared (a) CB-BTC, (b) CB/CN-BTC-350 and (c) CB/CN-BTC-450 catalysts.

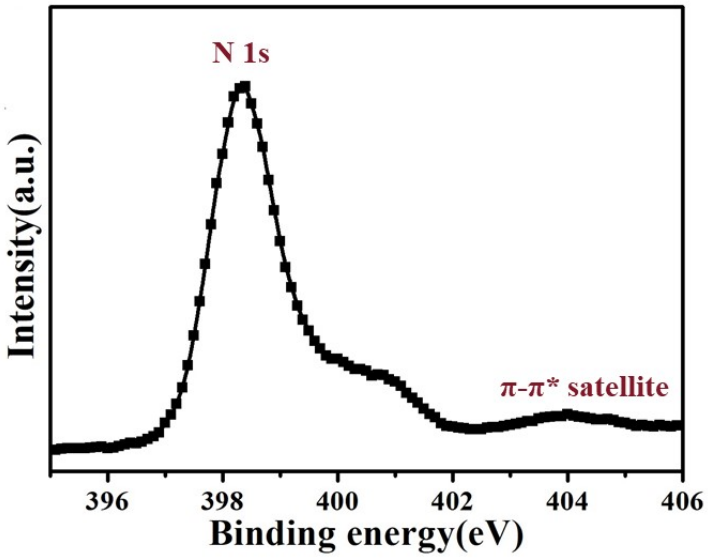

Fig. S5. XPS spectra of N 1s peaks of prepared CB/CN-BTC-350 catalyst.

3. Assessment of catalytic performance

3.1 General experimental procedure of ethynylation of formaldehyde

The ethynylation of formaldehyde catalyzed by the CB/CN-BTC-350 system under atmospheric pressure is detailed as follows. The other catalytic systems is analogous to the following:

Step 1: A quantity of 1.0 g of the CB/CN-BTC-350 catalyst and 20 mL of a 30% by mass fraction formaldehyde aqueous solution were introduced into a three-necked

round-bottom flask. The pH of the formaldehyde solution was adjusted to 7.5 using a 0.2 mol/L Na_2CO_3 solution. Subsequently, the mixture was treated with ultrasound for 10 minutes to ensure a homogeneous suspension.

Step 2: The air within the flask was purged with nitrogen (N_2), followed by the introduction of acetylene (C_2H_2). To activate the catalyst and form the Cu_2C_2 species, the mixture was magnetically stirred at 80 °C for 2 hour under a flow rate of 10 mL/min of C_2H_2.

Step 3: After catalyst activation, the ethynylation reaction proceeded at 90 °C for a duration of 10 hours. Once complete, the flow of C_2H_2 was replaced with N_2, and the reaction system was allowed to cool to room temperature.

Step 4: After reaction, the solution was centrifuged to separate the solid catalyst. The supernatant was then quantitatively analyzed using an Agilent 7890A gas chromatograph equipped with a DB-5 capillary column (dimensions: 0.32 mm × 50 m × 0.52 μm) and a flame ionization detector (FID). 1,4-Butanediol (BDO) served as the internal standard. Residual formaldehyde in the reaction solution was quantified via iodometry. The conversion of formaldehyde, yield of BYD, and selectivity of BYD were subsequently calculated based on the obtained data.

$$C_{HCHO}(\%) = \frac{m_0 - m}{m_0} \times 100\%$$

$$Y_{BYD}(\%) = \frac{M_{BYD} \times 2 \times 30}{m_0 \times 86} \times 100\%$$

$$S_{BYD}(\%) = \frac{Y_{BYD}}{X_{HCHO}} \times 100\%$$

m_0: Formaldehyde initial addition quality (g);

m: residual formaldehyde (g);

C_{HCHO}: conversion of formaldehyde (%);

M_{BYD}: mass of BYD (g);

Y_{BYD}: yield of BYD (%);

S_{BYD}: selectivity of BYD (%).

3.2 Optimization of reaction conditions

The low solubility of C_2H_2 in formaldehyde necessitates the use of C_2H_2 in excess to facilitate the ethynylation reaction. The synthesis of BYD can be efficiently achieved with a stoichiometric ratio of 1 mole of acetylene to 2 moles of formaldehyde. In the present study, trace amounts of propargyl alcohol were detected, and only a minimal portion of formaldehyde underwent polymerization to form paraformaldehyde.

3.3.1 Catalytic performance of different catalysts systems

Initial investigation into the catalytic activity for the ethynylation of formaldehyde were conducted by comparing the performance of different catalysts (Fig. S6). It was observed that the g-C_3N_4 carrier alone possessed no catalytic activity in the ethynylation reaction. The CB-BTC catalyst exhibited superior catalytic activity compared to CB, with an increase in formaldehyde conversion from 55.5% to 61.6% and an improvement in BYD yield from 35.6% to 46.5%. The incorporation of g-C3N4 into the catalyst structure significantly augmented its catalytic performance; CB/CN-BTC-350 achieved the highest formaldehyde conversion rate at 78.9%, alongside a BYD yield of 77.1% and selectivity of 97.7%. Conversely, CB/CN-BTC-450 displayed a diminished formaldehyde conversion of 69.4% and a decreased BYD yield of 61.4%.

Catalyst	C_{HCHO}/%	Y_{BYD}/%	***Catalyst***	C_{HCHO}/%	Y_{BYD}/%
Black	-	-	g-C_3N_4	-	-
CB	55.5	35.6	CB-BTC	61.6	46.5
CB/CN-BTC-350	78.9	77.1	CB/CN-BTC-450	69.4	61.4

Fig. S6 Evaluation of different catalysts systems.

3.2.2 Catalytic performance of different catalyst weight

Catalyst efficiency is typically influenced by the quantity of catalyst employed, with greater amounts generally leading to higher catalytic efficiency.[3] In this study, the ethynylation reaction using CB/CN-BTC-350 was conducted with varying amounts of catalyst (Fig. S7). The yield of BYD was found to be the lowest when the catalyst amount was 0.2 g. A significant increase in BYD yield was observed when the catalyst amount was raised from 0.2 g to 1.0 g. However, when the catalyst amount exceeded 1.5 g, there was negligible improvement in BYD yield. This can be attributed to the

limited number of formaldehyde and C_2H_2 molecules that can be adsorbed and activated by the catalyst at a low quantity of 0.2 g, resulting in a decreased production rate of BYD and consequently a lower yield. As the catalyst amount increased to 1.0 g, the frequency of contact between formaldehyde and C_2H_2 molecules on the catalyst surface increased, accelerating the reaction rate and enhancing the BYD yield from 20.7% to 77.0%. Beyond a certain threshold of catalyst usage, the reactive sites provided by the catalyst become saturated. At this point, other factors become limiting, and further increasing the amount of catalyst does not significantly enhance the yield of BYD.

Weight/g	C_{HCHO}/%	Y_{BYD}/%	**Weight/g**	C_{HCHO}/%	Y_{BYD}/%
0.2	21.2	20.7	0.5	53.4	51.8
1.0	78.5	77.0	1.5	79.5	77.3

Fig. S7 Evaluation of different catalyst weight.

3.2.3 Catalytic performance of different reaction temperature

Fig. S8 illustrates that the conversion of formaldehyde increased with an elevation in reaction temperature. However, there was a decline in BYD yield when the temperature rose to 95 °C. The optimal yield of BYD reached 77.2% at 90 °C. While higher reaction temperatures are favorable for accelerating the reaction rate, allowing for more BYD to be produced within a set timeframe, it is important to note that the formaldehyde acetylene reaction is exothermic.[4] Consequently, elevated temperatures do not encourage the chemical equilibrium to shift in the forward direction. Moreover, reactions conducted at 95 °C tend to generate a greater quantity of by-products compared to those at other temperatures.

Temperature/°C	C_{HCHO}/%	Y_{BYD}/%	***Temperature/°C***	C_{HCHO}/%	Y_{BYD}/%
80	61.9	60.6	85	72.1	70.5
90	78.7	77.2	95	82.4	76.1

Fig. S8 Evaluation of different temperature.

3.2.4 Catalytic performance of different formaldehyde concentration

Fig. S9 demonstrates that the yield of BYD increases with the augmentation of formaldehyde content in the aqueous solution when the initial mass fraction of

formaldehyde is below 25%. This phenomenon may be attributed to the diminished formaldehyde content, which impedes the reduction process of the catalyst. Consequently, the catalyst does not achieve full activation during the reaction, resulting in a lower BYD yield after a 10-hour reaction period. Additionally, at lower formaldehyde concentrations, the adsorption of formaldehyde molecules onto the catalyst surface is inadequate, leading to a reduced BYD yield over a specific time frame. The highest BYD yield of 77.2% was attained when the initial formaldehyde content in the aqueous solution was 25%. However, when the initial mass fraction of formaldehyde in the aqueous solution exceeds 25%, the BYD yield decreases with further increases in the initial formaldehyde content. This primarily stems from the solvent effect, where formaldehyde molecules undergo polycondensation within the reaction system to form various polyformaldehyde hydrates. Generally, formaldehyde polymers manifest as white crystals, which can obstruct the catalyst pores and subsequently diminish catalyst activity.

Concentration/%	C_{HCHO}/%	Y_{BYD}/%	***Concentration/%***	C_{HCHO}/%	Y_{BYD}/%
15	62.8	61.4	20	72.2	70.7
25	78.7	77.2	30	74.8	72.0

Fig. S9 Evaluation of different formaldehyde concentration.

3.2.5 Catalytic performance of different reaction time.

As shown as Fig. S10, the influence of reaction duration on the ethynylation of formaldehyde was investigated over a range from 4 to 15 hours. The yield of BYD progressively increased from39.3% to 81.5%. Notably, when the reaction time reached 12 hours, the rate of BYD yield growth slowed, while the selectivity experienced a slight decline.

Time/h	C_{HCHO}/%	Y_{BYD}/%	***Time/h***	C_{HCHO}/%	Y_{BYD}/%
4	40.1	39.3	6	56.7	55.0
8	69.1	67.6	10	78.7	77.2
12	82.4	79.9	15	84.3	81.5

Fig. S10 Evaluation of different reaction time.

3.3 Stability of catalyst

In multi-phase reactions, heterogeneous catalysts typically offer the advantage of recyclability.[5] In this study, post-reaction catalyst were subjected to a thorough cleaning process, involving rinsing with water, washing with ethanol, and subsequent drying under low temperature and vacuum conditions. These treated catalysts were then reused under identical conditions for subsequent reactions. The impact of catalyst stability on the yield of BYD was examined.

Fig. S11 shows that CB/CN-BTC-350 is more stable than CB/-BTC. Over six cycles, the BYD yield on CB/BTC decreased from 46.5% to 32.7%, and the formaldehyde conversion dropped from 62.4% to 47.3%. In contrast, the BYD yield of CB/CN-BTC-350 remained at 73.1% even after six cycles, and the formaldehyde conversion and BYD selectivity remained above 76.7% and 95.3%, respectively, during the same period. The stable interaction between CuO and g-C_3N_4 enhances the stability of the active Cu^+ species under reducing conditions. This finding supports the observed high stability in CB/CN-BTC-350.

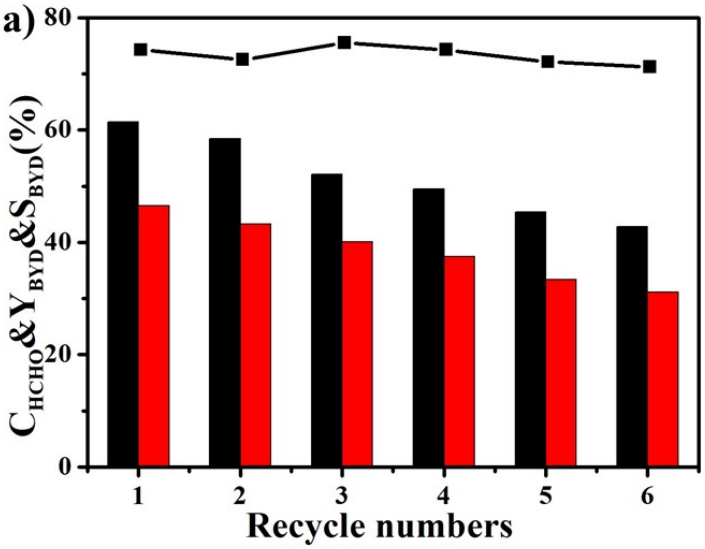

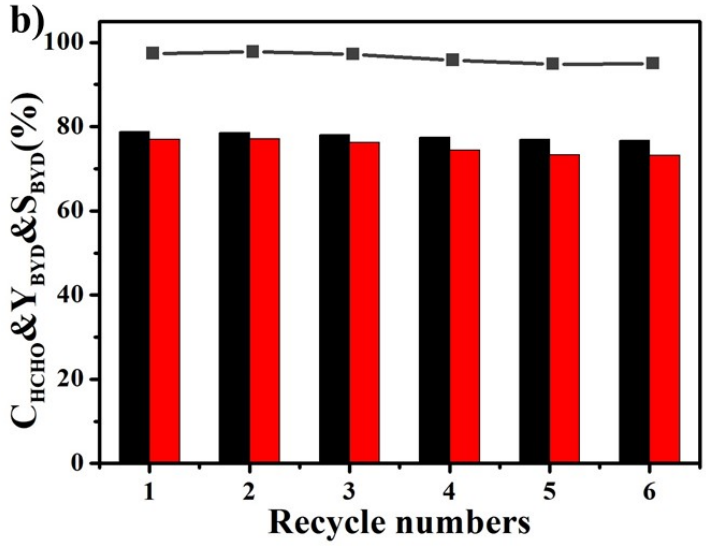

Fig. S11. Cycle stability of (a) CB-BTC and (b) CB/CN-BTC-350 catalyst for the ethynylation of formaldehyde reaction.

The study analyzed the stability of the catalyst C/CN-BTC-350. As shown in Fig. S12, the BYD yield on C/CN-BTC-350 decreased from 72.3% to 59.7% over five cycles. The study suggests that the co-catalyst Bi_2O_3 in the CB/CN-BTC-350 catalyst promotes the dispersion of CuO NPs. Moreover, the CuO- Bi_2O_3 interaction stabilizes Cu^+, which is important for the catalytic efficiency and stability in the ethynylation of formaldehyde for BYD synthesis.

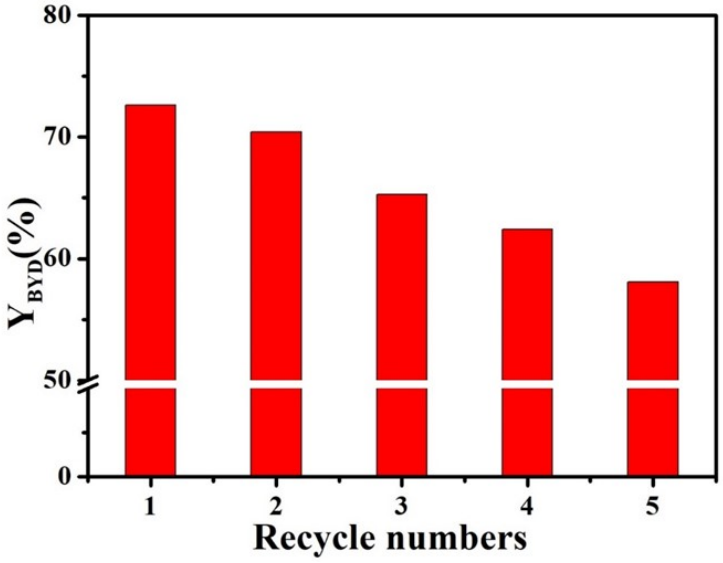

Fig. S12 Cyclic catalytic performance of C/CN-BTC-350 catalyst.

4. Kinetic analysis for the ethynylation reaction

The kinetic analysis of the ethynylation reaction was conducted in accordance with the standard experimental protocol. At 10 seconds post-reaction initiation, a sample equivalent to 2% of the total reaction volume was extracted and dissolved in 0.5 mL of BDO. This procedure was repeated at subsequent intervals throughout the reaction (i.e., 1 hour, 2 hours, 4 hours, 6 hours, 8 hours, and 10 hours). The resultant samples were filtered to remove any insoluble substance to injection into the GC for analysis.

In line with the characteristics of the ethynylation reaction, kinetic equation 1 was established.[6] The apparent activation energy was subsequently calculated using the pertinent equations.[7] By taking the logarithm of the reaction rate as presented in equation 1, equation 2 was derived. Given that C_2H_2 is used in excess, the value of β is set to zero, thus yielding equation 3. Equation 3 was then integrated with the Arrhenius equation (equation 4). This integration allows for the measurement of the BYD concentration, as depicted in Fig. S13-S15, alongside the formaldehyde concentration at various reaction times and corresponding temperatures. This data enables the determination of the relationship between the rate of change of BYD concentration over time (dC_{BYD}/dt) and the concentration of formaldehyde (C_{HCHO}), leading to the calculation of the natural logarithm of the rate constant (ln K) from the intercept. Consequently, the relationship between ln K and the inverse of temperature (1/T) can be established. From equation 4, the activation energy associated with the ethynylation of formaldehyde over different catalysts can thus be determined.

$$\gamma_B = dC_{BYD}/dt = K \times C_F^{\alpha} \times C_A^{\beta} \quad (1)$$

$$\ln(dC_{BYD}/dt) = \ln K + \alpha \ln(C_{HCHO}) + \beta \ln(C_{C2H2}) \quad (2)$$

$$\ln(dC_{BYD}/dt) = \ln K + \alpha \ln(C_{HCHO}) \quad (3)$$

$$\ln k = \ln A + Ea/RT \quad (4)$$

K: reaction rate constant;

A: pre-exponential factor;

α and β: orders of reaction;

C_{BYD}: concentration of 1,4-butynediol (mol/L);

C_{HCHO}: concentration of formaldehyde (mol/L).

C_{C2H2}: concentration of acetylene (mol/L).

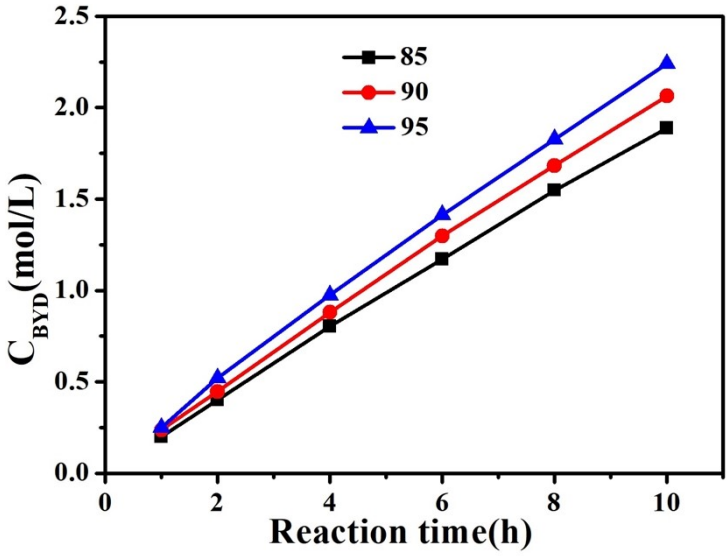

Fig. S13. Variation of BYD concentration (C_{BYD}) with reaction time over CB-BTC catalyst.

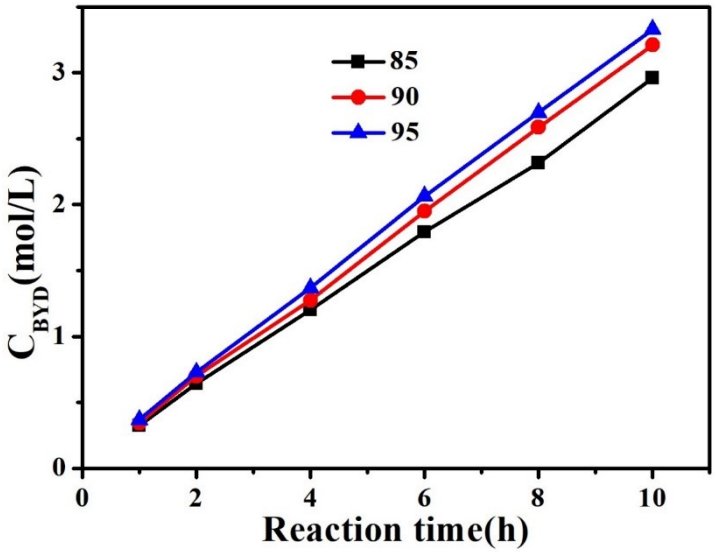

Fig. S14. Variation of BYD concentration (CBYD) with reaction time over CB-BTC-350 catalyst.

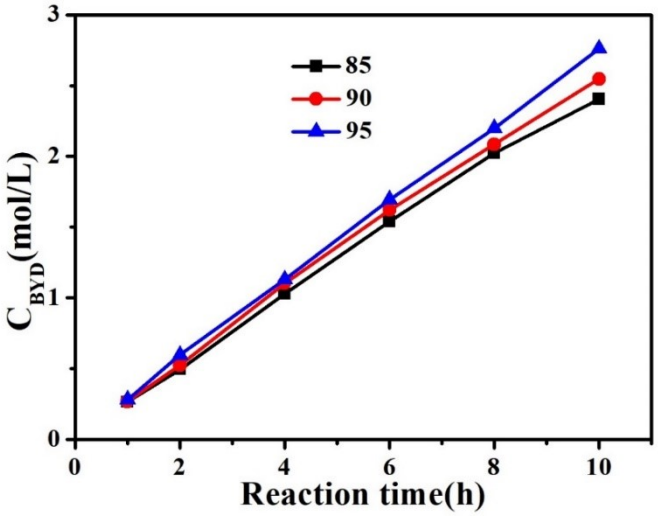

Fig. S15 Variation of BYD concentration (CBYD) with reaction time over CB-BTC-450 catalyst.

5. Mechanism of CB/CN-BTC catalyst

Fig. S16 shows the progressive formation of CuC≡CCu, which is confirmed by XRD analysis taken at different times during the activation procedure in the formaldehyde/acetylene system. After approximately 150 minutes, the characteristic diffraction peaks of CuO disappeared, and new diffused diffraction peaks suggests that CuO underwent a phase change, resulting in the formation of a new species, which is believed to be an amorphous active cuprous acetylide (CuC≡CCu).[8] Furthermore, no excessive reduction product (Cu^0) was detected in the sample.

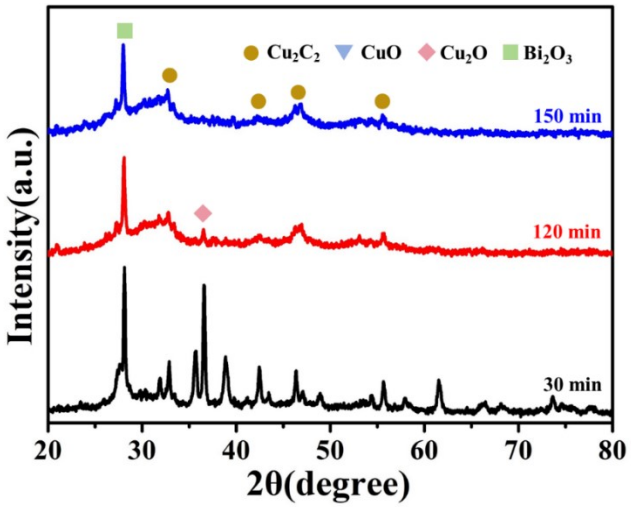

Fig. S16 XRD patterns of CB/CN-BTC-350 during activation procedure in formaldehyde/acetylene system.

Furthermore, the activation process for the CB/CN-BTC-350 catalyst was also carried out in a formaldehyde system. As shown in Fig. S17, the XRD patterns of the tested catalyst remained consistent with each other at different times. This indicates that no phase transition or significant structural changes occurred in CB/CN-BTC-350 after the activation process in the formaldehyde system.

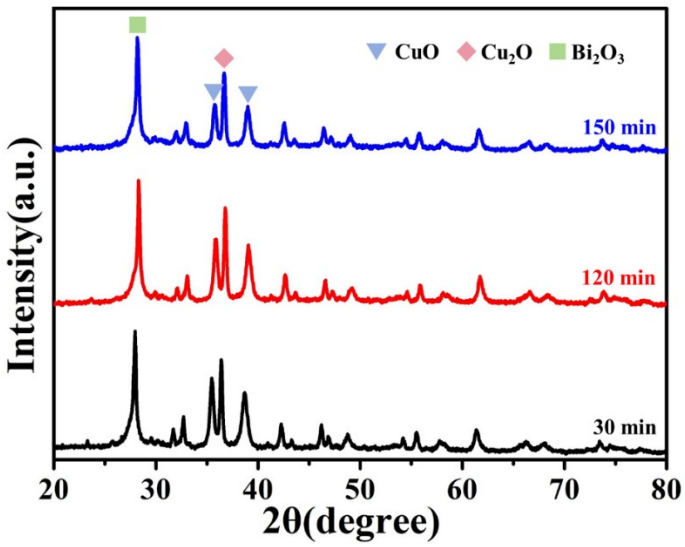

Fig. S17 XRD patterns of CB/CN-BTC-350 during activation procedure in formaldehyde system.

Moreover, chemical state of Cu species in CB/CN-BTC-350 after activation in the formaldehyde/acetylene system was analyzed using XPS. As shown as Fig S18, the Cu 2p spectrum of the catalyst showed peaks at 933.2 eV and 953.4 eV, indicating the presence of a single oxidation state of Cu^{+}.[9] This suggest that the chemical state of Cu species changed during the reaction, possibly due to the transformation of Cu^{2+} into Cu^{+} or Cu^{0}. The Cu LMM XAES spectra were obtained due to the overlap of the Cu^{+} and Cu^{0} peaks in the XPS spectra. Fig. S19 shows that the catalyst presented symmetrical broad peak at approximately 915.5 eV, which was attributed to Cu^{+} species.[10] No peak corresponding to Cu^{0} (917.5 eV) was observed in the catalyst, indicating the absence of Cu^{0} in the activated catalysts.

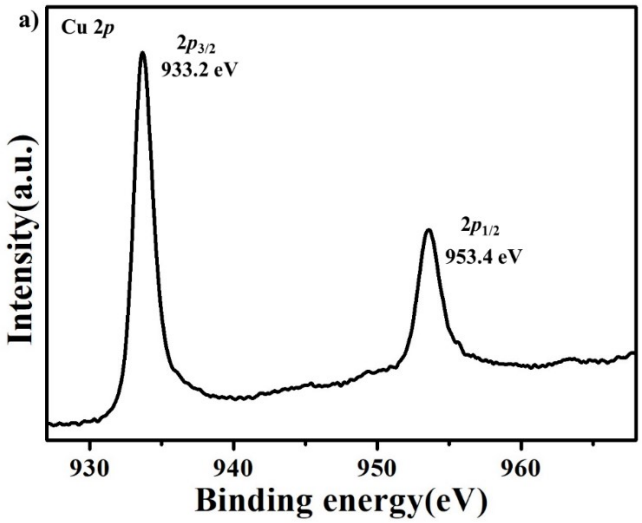

Fig. S18 Cu 2p XPS spectra of CB/CN-BTC-350 after activation.

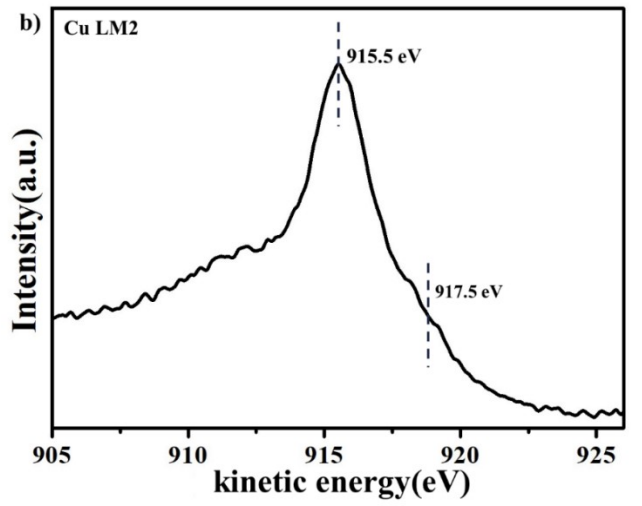

Fig. S19 Auger Cu LMM XPS spectra of CB/CN-BTC-350 afteractivation.

To elucidate the catalytic differences across various activation systems, the activation behavior of CB/CN-BTC-350 was investigated in two distinct settings: the formaldehyde system and the formaldehyde/acetylene system. These studies were conducted independently to discern the specific influences of each reaction environment on catalyst performance.

Activation of catalyst in formaldehyde system

The activation procedure for the CB/CN-BTC catalyst in the formaldehyde system involved submerging the catalyst in a formaldehyde solution and heating it under a nitrogen atmosphere at 90 °C for a duration of 2 hours. Upon completion of the

activation process, the catalyst was allowed to cool, subsequently filtered, and finally dried under vacuum at 25°C for a period of 24 hours. The resulting activated catalyst was designated as CB/CN-BTC-F.

Activation of catalyst in formaldehyde/acetylene system

The activation of the CB/CN-BTC catalyst in the formaldehyde/acetylene system was conducted by immersing the catalyst in a formaldehyde solution and exposing it to an acetylene atmosphere at 90°C for 2 hours. Post-activation, the catalyst was cooled, filtered, and then desiccated under vacuum at 25°C for 24 hours. The activated catalyst obtained from this process was designated as CB/CN-BTC-F/A.

The activated catalysts, CB/CN-BTC-F and CB/CN-BTC-F/A, were each employed in the ethynylation reaction of formaldehyde. Initially, a nitrogen atmosphere was established until the reaction temperature reached 90°C, at which point it was switched to an acetylene gas environment to facilitate further reaction. After a 10-hour duration, the reaction mixture was cooled and filtered, and the BYD content within the solution was quantitatively analyzed. As indicated in Table S4, the CB/CN-BTC catalyst that underwent direct activation in the formaldehyde/acetylene system exhibited superior formaldehyde conversion efficiency, as well as enhanced BYD yield and selectivity. In comparison, when the catalyst was activated using only formaldehyde, it demonstrated diminished ethynylation activity.

Table S4 Evaluation results of the catalysts

Catalyst	C_{HCHO}/%	Y_{BYD}/%	S_{BYD}/%
CB/CN-BTC-F	62.7	51.5	82.1
CB/CN-BTC-F/A	80.6	78.6	97.5

Based on the aforementioned findings, in the absence of acetylene, CuO present within the CB/CN-BTC cannot completely reduced to Cu_2O by formaldehyde. In the presence of acetylene, the CuO within the CB/CN-BTC catalyst is likely converted into copper acetylide species, which exhibit high reactivity towards acetylene reactions.[11] When the activated CB/CN-BTC-F catalyst was introduced into the reaction system, it also underwent transformation into active cuprous species.[12] The primary reasons for

this are as follows: (1) The formaldehyde leads to a depletion of copper species (with the copper content decreasing from 42.7% to 38.9%), consequently diminishing the number of active sites generated; (2) The crystalline Cu_2O species also impede the formation of active cuprous species. These results further suggest that the transformation of CuO species into an acetylene-active center should optimally occur under the combined influence of formaldehyde and acetylene, a process that is more effective than the reduction of CuO first to Cu_2O then followed by the formation of active cuprous species later.

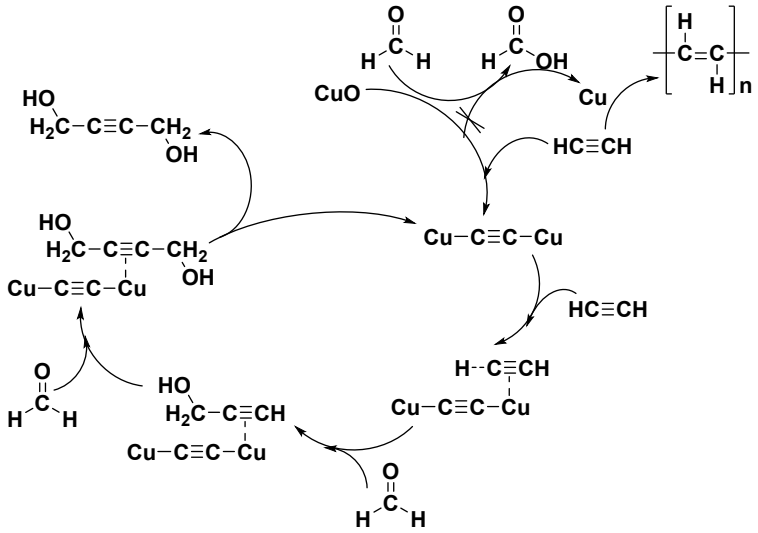

Fig. S20. Possible ethynylation mechanism over the Cu-based catalyst surface.

Table S5 Activity of different Catalysts for ethynylation of formaldehyde

Catalyst	Conditions	C_{HCHO}(%)	Y_{BYD}(%)	S_{BYD}(%)	Reference
30Cu15Zn/SiO_2	1.2 g/20 mL (20 wt %)	72	72	100	12
16Au@Cu_2O	250 mg/5 ml (35 wt%)	-	65.8	-	13
CuO-ZnO	2.5 g/50 mL (35 wt %)	-	70.9	-	14
Cu_xO-Fe_yO_z	2.5 g/50 mL (35 wt %)	-	59.83	-	15
CuO/MgO	1.2 g/20 mL (20 wt %)	63	39	62	16
CuO/MnO_x-15	1.2 g/20 mL (20 wt %)	79	76	96	16
CuBi/MCM-41	1.2 g/20 mL (20 wt %)	57	53	93	17
$Cu_{0.84}Al_{0.16}$	2.5 g/50 mL (35 wt %)	-	68	-	4
CuO/MgO-SiO_2	0.5 g/10 mL (28 wt %)	-	67.2	-	18
CB/CN-BTC-350	1.0 g/20 mL (30 wt %)	78.9	77.1	97.7	This work

References

1. X. P. Yan, M. L. Zhang, Y. Z. Chen, Y. H. Wu, R. Z. Wu, Q. Wan, C. X. Liu, T. T. Zheng, R. J. Feng, J. Zhang, C. J. Chen, C. Xia, Q. G. Zhu, X. F. Sun, Q. L. Qian and B. X. Han, A*ngew. Chem., Int. Ed.*, 2023, **62**, e202301507.

2. S. S. Y. Chui, S. M. F. Lo, J. P. H. Charmant, A. G. Orpen and I. D. A Williams, *Science*, 1999, **283**, 1148-1150.

3. C. Vogt and B. M. Weckhuysen, *Nat. Rev. Chem.*, 2022, **6**, 89-111.

4. Z. P. Wang, L. J. Ban, P. F. Meng, H. T. Li and Y. X. Zhao, *Nanomaterials*, 2019, **9**, 1038.

5. C. M. Friend and B. J. Xu, *Acc. Chem. Res.,* 2017, **50**, 517-521.

6. S. Sato, *Chem. Phys*., 2016, **469-470**, 49-59.

7. Q. R. S. Miller, J. P. Kaszuba, H. T. Schaef, M. E. Bowden, B. P. McGrail and K. M. Rosso, *Chem. Commun.,* 2019, **55**, 6835-6837.

8. Z. P. Wang,Z. Z. Niu,Q. A. Hao,L. J. Ban,H. T. Li,Y. X. Zhao and Z. Jiang, *Catalysts*, 2019, **9**, 35.

9. D. Ferrah, A. R. Haines, R. P. Galhenage, J. P. Bruce, A. D. Babore, A. Hunt, I. Waluyo and J, C. Hemminger, *ACS Catal*., 2019, **9**, 6783-6802.)

10. J. Kim, W. Choi, J. W. Park, C. Kim, M. J. Kim and H. Song, *J. Am. Chem. Soc*., 2019, **141**, 6986-6994.

11. T. Bruhm, A. Abram, J. Häusler, O. Thomys and K. Köhler, *Chem. Eur. J.*, 2021, **27**, 16834-16839

12. G. H. Yang, L. X. Yang and J. L. Chen, *Ind. Eng. Chem. Res.*, 2023, **62**, 21067-21077.

13. X. Huang, H. T. Li, B. Zhang, Y. Zhang, H. Wang, L.J. Ban, Y. X. Xu and Y. X. Zhao, *Nanoscale*, 2024, **16**, 1971-1982.

14. L. J. Ban, H. T. Li, Y. Zhang, R. F. Wu, X. Huang, J. H. Zhao and Y. X. Zhao, *J. Phys. Chem. C*, 2021, **125**, 16536-16549

15. H. T. Li, L. J. Ban, Z. Z Niu, X. Huang, P. F. Meng, X. D. Han, Y. Zhang, H. X. Zhang and Y. X. Zhao, *Nanomaterials*, 2019, **9**, 1301.

16. G. H. Yang, F, Gao, L, X. Yang and J. D. Wang, *React. Kinet. Mech. Cat*., 2022, **135**, 2611-2627.

17. G. H. Yang, Y. M. Yu, M. U. Tahir, S. Ahmad, X. T. Su, Y. H. Xie and J. D. Wang, *React. Kinet. Mech. Cat*., 2019, **127**, 425-436.

18. Z. P. Wang, L. J. Ban, P. F. Meng, H. T. Li and Y. X. Zhao, *Nanomaterials*, 2019, **9**, 1137.